COMMUNICATION

Check for updates

The regulation effect of coordination number on the conductance of single-molecule junctions†

Qiang Wan, ‡[a] Hong-Yang Guo,‡[a] Yi-Fan Zhou,[a] Jia-Nan Jiang,[a] Wenbo Chen, *[b] Ju-Fang Zheng,[a] Yong Shao,[a] Ya-Hao Wang *[a] and Xiao-Shun Zhou *[a]

Combining the STM break junction technique and theoretical simulation, we report that the presence of multiple anchoring sites leads to different configurations of single-molecule junctions by changing the interfacial coordination numbers. These distinct variations in electronic structures cause their conductance to change by about 2500-fold.

Introduction

As the size of traditional silicon-based electronic devices continues to decrease to a few nanometers scale, the presence of the quantum effect significantly alters their properties.[1–3] Consequently, the bottom-up approaches to building functional components using chemically identical molecules are considered a promising approach for future nanoelectronics.[4–7] This primarily requires constructing robust metal–molecule–metal junctions to explore their electron transport properties at the single-molecule level.[8–10] Benefiting from the rapid development of nanotechnology and instrumentation, many experimental techniques have been developed in the past three decades to construct single-molecule junctions and measure their conductance, such as the widely used mechanically controllable break junction (MCBJ) and scanning tunneling microscopy break junction (STM-BJ).[11–15] In these measurements, extensive processes have been achieved in the understanding of electron transport in single-molecule junctions.[16–18] For example, the nature of metal molecule contact has a great impact on the stability, binding configuration, interface coupling and energy level arrangement of single-molecule junctions.[19–26] However, the molecular adsorption and the arrangement of the atoms at the metallic electrode interfaces are *a priori* unknown. Uncovering such metal–molecule[27] contacts in the structure–activity relationships of single-molecule junctions remains a great challenge.[28–32]

To enhance chemical and mechanical stability as well as electronic coupling, molecules with multidentate anchoring groups or multiple anchoring units have recently been designed and synthesized for constructing molecular junctions.[33–37] For example, Kiguchi *et al.* found that single-molecule junctions consisting of a quarter-thiophene-based molecule present three conductance values, and claimed that various conductance values within one molecule can be attributed to the shift of anchors.[38] Hong *et al.* reported the regulation of conductance *via* alternating anchoring sites through mechanical control.[39] Venkatraman *et al.* reported four conductance values within a single molecular scaffold, which originated from distinct combinations between the electrodes and bis-terpyridine-based molecule.[40] Furthermore, these molecular components with multiple contact sites enable mechanically induced changes of coordination numbers at the metal–molecule interface. However, the molecules involved in these investigations are relatively complex, and the complicated mechanism of the impact of molecular coordination number on conductance remains unclear. Therefore, it is necessary to clarify how the number of anchoring sites affects the conductance of single-molecule junctions composed of a simple molecular backbone, which will shed light on conductance regulation and molecular device design.

Molecules composed of nitrogen-based heterocycles could strongly interact with the Au electrode, which has been extensively studied in the past,[41–43] and is suitable for elucidating the correlation between the anchor site number and conductance of the molecular junction. Herein, in conjunction with STM-BJ measurements and density functional theory (DFT) calculations, we use 1-(4-imidazol-1-ylphenyl)imidazole (denoted as **N1**) and 4,4′-(1,4-phenylene)bis(4*H*-1,2,4-triazole) (denoted as **N2**) as model molecules to investigate their charge transport

[a] Key Laboratory of the Ministry of Education for Advanced Catalysis Materials, Institute of Physical Chemistry, Zhejiang Normal University, Jinhua 321004, China. E-mail: yahaowang@zjnu.edu.cn, xszhou@zjnu.edu.cn

[b] Shanghai Key Laboratory of Materials Protection and Advanced Materials in Electric Power, Shanghai University of Electric Power, Shanghai, China. E-mail: wenbochen@shiep.edu.cn

† Electronic supplementary information (ESI) available. See DOI: https://doi.org/10.1039/d3tc03618a

‡ These authors contributed equally.

Fig. 1 Schematic of coordination numbers induced by various conductance states of single-molecule junctions for **N1** and **N2** molecules.

properties. Molecule **N1** possesses one anchoring site bonding to electrodes, while molecule **N2** possesses two triazole rings located at both ends with each triazole ring providing two anchoring sites. As schematically shown in Fig. 1, **N2** in molecular junctions can be anchored between Au electrodes *via* one–one (**1–1**), one–two (**1–2**) and two–two (**2–2**) modes. Such a regulating effect of molecule–metal coordination numbers on single molecule conductance was investigated. The results show that the **N1** molecule possesses single conductance values, while the **N2** molecule possesses three. Moreover, different coordination numbers of **N2** lead to different binding strengths and unoccupied states, further regulating its conductance. This work reveals the impact of the coordination number of the molecule backbone on conductance, providing physical insights and potential strategies for engineering the conductance of single-molecule junctions *via* molecular design.

Results and discussion

The conductance of the single molecular junction of **N2** was first characterized by the STM-BJ technique in dodecane containing 0.1 mM **N2** molecule. The Au (111) substrate was polished and annealed before each STM experiment. The typical individual conductance trace for **N2** obtained in dodecane at a bias voltage of 100 mV is shown in Fig. 2a. As the nanogap between the two electrodes increases by withdrawing the tip, the conductance decreases and presents three plateaus (located at about $10^{-1.6}$, $10^{-3.5}$, and $10^{-5.0}$ G_0, where G_0 is the quantum conductance equalling ~ 77.5 μS), suggesting successful construction of molecular junctions. Besides, the presence of high, medium and low conductance (denoted as HC, MC and LC, respectively) suggests a potential application in molecular devices due to its distinct variation between different states (HC:LC = $10^{3.4}$). Accordingly, it can be found from the one-dimensional (1D) conductance histogram (Fig. 2b) that three obvious conductance peaks (Gaussian fitting) of the **N2** junction are located at $10^{-1.6}$, $10^{-3.5}$, and $10^{-5.0}$ G_0, which are in agreement with the results from typical conductance traces (Fig. 2a). The most probable absolute

Fig. 2 (a) Typical conductance-distance traces of a single molecular junction, (b) one-dimensional (1D) conductance histogram and (c) two-dimensional (2D) conductance histogram as a function of relative displacement for **N2**. (d) 1D conductance histogram for **N1**.

displacement for molecular junctions is about 1 nm (Fig. S1, ESI†), which is comparable with the molecular length of **N2** (Fig. S2, ESI†). This further confirms the formation of single-molecule junctions. Furthermore, the two-dimensional (2D) conductance histogram in Fig. 2d also shows the corresponding three stretching states of HC, MC and LC in statistical analysis of relevant displacements of each conductance curve from $10^{-6.0}$ G_0 to $10^{-0.3}$ G_0.

As aforementioned, the **N2** molecule possesses two sites to anchor each electrode, which can lead to three different configurations of **1–1**, **1–2**, and **2–2** with different coordination numbers at the interfaces. This might present three stable conductance values. To further verify this conjecture, we studied the conductance of single-molecule junctions with less anchoring sites, *i.e.*, the **N1** molecule. In comparison to the **N2** molecule, the **N1** molecule possesses two imidazole rings located at the *para*-site of benzene instead of a triazole ring, thus only contributing one anchoring site at each end of the **N1** molecule (**1–1**).

As shown in Fig. 1d, only one stable peak with Gaussian fitting appears at $10^{-4.5}$ G_0, which is in agreement with the location of the plateau in the representative conductance-distance traces (Fig. S2a, ESI†). The formation of single-molecule junctions is also confirmed in the 2D conductance histograms (Fig. S2b and c, ESI†). Thus, the presence of a single conductance peak proves that fewer anchoring sites lead to relatively specific configurations of single-molecular junctions, in comparison to diverse configurations of **N2**-based single-molecule junctions. To gain further physical insight into the effect of the number of anchoring sites on conductance, we carried out DFT calculations to investigate the interaction between **N2/N1** with the Au electrodes by various configurations,

This journal is © The Royal Society of Chemistry 2024

J. Mater. Chem. C, 2024, **12**, 60–65 | **61**

Fig. 3 (a) Optimized configuration (upper panel) of the **N2** molecular junction with different anchoring states, and corresponding charge density difference plots ($\rho_{diff} = \rho_{A-B} - \rho_A - \rho_B$, lower panel). The isovalue of electron density was set to 0.02 e Å^{-3}, the purple region represents the depletion of electrons, while the red region represents accumulation after **N2** adsorption. (b) Calculated partial density of states (PDOS, the Fermi level was set to 0 eV) of the **N2** molecule and (c) transmission spectra in various anchoring states.

as well as the corresponding electronic structures and conductance. Optimized structures for **N2** molecule anchoring between two Au electrodes *via* **1–1**, **1–2** and **2–2** modes are shown in Fig. 3a (upper panel), respectively.

The average bond length of two Au–N bonds in **1–1** is 2.18 Å, showing the adsorption energy of −2.46 eV. For the anchored **N2** molecule in **1–2** mode, the average Au–N bond is 2.23 Å, and the corresponding adsorption energy is −2.66 eV, which is lower than that of the **1–1** mode. As the coordination number of the **N2** molecule to gold electrodes continues to increase and reaches a maximum, all two anchoring sites at each end of the molecule bond to the gold electrode. In this case, the average Au–N bond length is 2.23 Å, and the adsorption energy further decreases to −2.88 eV. Besides, the charge density difference plots (lower panel of Fig. 3a) show that a larger coordination number results in stronger electron transfer. Taking the **2–2** and **1–1** modes as examples, there are obvious regions of electron transfer on the benzene rings in the **2–2** case, while in the **1–1** case, the electron gains and losses mainly take place on the triazole ring. The above results indicate that the interaction between the **N2** molecule and electrodes was strengthened when the coordination number increased, leading to stronger binding and wider regions of changes in electron density.

PDOS of **N2** in various anchoring configurations are investigated to analyse their differences in terms of electronic structure, and the results are shown in Fig. 3b. One can find that the unoccupied states closest to the Fermi level obviously shift towards lower energy, and even straddle across the Fermi level when **N2** connects with electrodes in a **2–2** mode, suggesting that the states start to be partially filled as the coordination number increases, which would facilitate the electron transfer and improve the conductance. Therefore, we calculated the transmission spectra for single-molecule junctions with these

three modes, and the results are shown in Fig. 3c. The location of the peak closest to the Fermi level shows the same trend as that shown in PDOS, *i.e.*, increasing coordination number leads to the shift of the conductance peak towards lower energy. The order of the conductance values for **N2** in various modes is **2–2** > **1–2** > **1–1**, corresponding to experimentally observed HC, MC and LC, respectively.

In addition, the conductance of another single-molecule junction configuration for **N2** in a **1–1** mode has been examined (Fig. S3, ESI†). The results reveal that their conductance values are comparable regardless of whether the two anchoring sites are on the same side or opposite sides. We also simulated the single-molecule junction configuration of **N2** in a different nanogap, which exposes extra sites for connecting electrodes. The results suggest that their conductance values are comparable (Fig. S4, ESI†), excluding the possibility that other anchoring modes may contribute to different conductance values. Besides, experiments and calculations exclude the contributions of the configuration of internal N binding to Au and the configuration of two N in the same ring binding to Au and to the HC of the **N2** molecular junction (Fig. S5, ESI†).

Now, it is clear that the presence of multiple anchoring sites of **N2** leads to the formation of diverse single-molecule junctions. Increasing the coordination numbers can improve the single-molecule conductance value by about three orders of magnitude. We also further compare the chemical and mechanical stability by analysing the junction formation statistics. In order to statistically represent this complex data set, the results obtained from these over 1000 traces in each curve were individually analysed. As summarized in the diagrams shown in Fig. 4a, it was found that almost 83.2% of the conductance traces exhibited plateau-like events assigned to the formation of molecular junctions for **N2**, compared to 61.7% for **N1**. This indicates that the multiple N anchoring sites can also significantly promote the metal–molecule contacts and interactions.

Furthermore, we count the number of occurrences of HC, MC and LC plateaus in all the plateau-even curves of **N2** to analyse the molecular junction formation mechanism. Their relative count ratios are shown in Fig. 4b. It can be found that the **1–2** configuration for MC dominates the withdrawal process of the tip from the substrate. There might be two reasons: (I) the pre-adsorbed **N2** molecules on the Au substrate prefer two N to bind simultaneously. This leads to the formation of **1–2** and **2–2** configurations when the tip is withdrawn from the SAMs; (II) the **2–2** configurations can evolve into a **1–2** configuration during the tip withdrawing process. In addition, it is also found that there were almost exclusively LC plateau-like events in all conductance-distance traces. This indicates that the **1–1** configuration is almost evolved from the **1–2** and **2–2** configurations. Thus, the molecular junction formation process and mechanism are schematically summarized in Fig. 4c. The 1D and 2D conductance histograms from the selected conductance-distance traces display the LC, MC, or HC steps, and all show the three conductance peaks (Fig. S6, ESI†), indicating that all or two of the three type steps appear
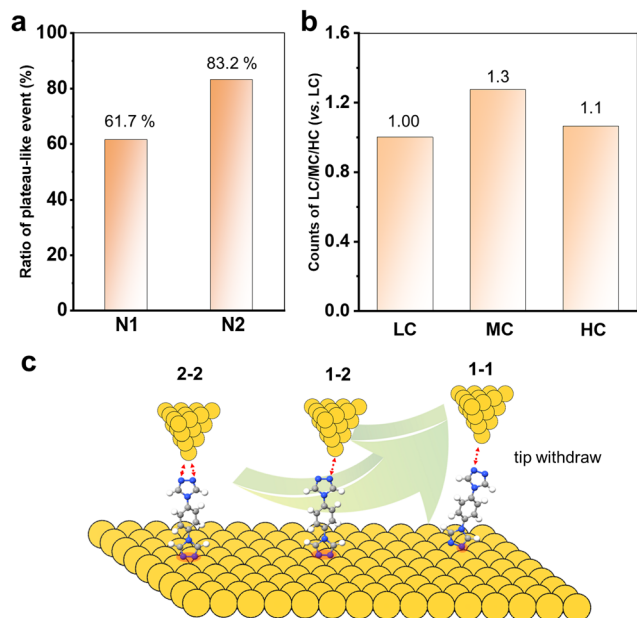
62 | *J. Mater. Chem. C*, 2024, **12**, 60–65

This journal is © The Royal Society of Chemistry 2024

Fig. 4 (a) The percentage of plateau-like events in the conductance traces for **N1** and **N2**. (b) Relative count ratios of LC, MC and HC plateau-like events for **N2**. (c) Schematic of the molecular junction formation mechanism during withdrawing the tip from the substrates with adsorption of **N2**.

simultaneously in most of the conductance-distance traces. This further supports that a **2–2** or **2–1** configuration of the molecular junction is firstly formed when the tip is driven into the SAM of **N2** with both N binding to the Au substrate. The molecules with multiple anchoring sites offer a unique opportunity to tune the conductance of single-molecule junctions for the design of molecular devices.

Conclusions

In summary, we have successfully investigated the effects of the coordination numbers of molecule–metal contacts on charge transport by using the STM-BJ technique and theoretical calculations. The **N2** molecule has two anchoring sites at each end, exhibiting three stable conductance values. Combined with the theoretical investigations, we revealed that the three HC, MC and LC values of **N2** were attributed to coordination numbers of **2–2**, **1–2** and **1–1** between **N2** and the two Au electrodes. The coordination number between a molecule and electrodes distinctly affects the binding strengths of molecules and plays a crucial role in tuning their electronic structure which can change the conductance of single-molecule junction more than three order of magnitude. Our work provides a clear and constructive perspective for developing electronic components with multiple anchoring sites.

Experimental section

Conductance measurements

Single-molecule conductance measurements by using an STM break-junction (STM-BJ) were carried out using a home-modified Nanoscope IIIa STM (Veeco, US). The naturally formed (111) facet at a Au bead substrate and mechanically-cut Au tip (0.25 mm diameter, 99.999%, Alfa Aesar) were used as two working electrodes. Prior to each experiment, the Au(111) substrate was subjected to electrochemical-polishing and flame-annealing. The single-molecule conductance measurements were performed in a dodecane solution containing 0.1 mM target molecules. 1,4-Bis (1*H*-pyrazol-4-yl) benzene (95% +), 4,4′-(1,4-phenyl) bis (4*H*-1,2,4-triazole) (98%), and 1-(4-imidazol-1-ylphenyl)imidazole (98%) were purchased from Jilin Chinese Academy of Sciences-Yanshen Technology Co., Ltd. (Jilin, China).

The process of the STM-BJ method is briefly described as follows: first, the STM tip is driven toward the substrate to a preset current value (50 nA) through piezoelectric control. An external pulse voltage is then applied to the z-piezo to bring the STM tip into the substrate surface to softly contact with the substrate. The tip is then pulled away from the substrate at a constant speed of 20 nm s^{-1}. During this process, single molecular junctions can be formed. Simultaneously, the current at the tip was recorded at a sampling rate of 20 kHz. Thousands of tip current–displacement curves were collected to construct conductance histograms without data selection. Conductance measurements were performed at a bias voltage of 100 mV.

Computational details

All structural relaxation of molecules and single-molecule junctions using an FHI pseudopotential and double-zeta polarized (DZP) basis set within the generalized gradient approximation (GGA) with the Perdew–Burke–Ernzerhof (PBE) functional were performed by the QuantumATK (S-2021.06-SP1) package.[44–46] For structural relaxation of the central region of the devices, the convergence criterion of force was set to 0.01 eV Å^{-1}, and a $2 \times 2 \times 1$ Monkhorst–Pack grid with a density mesh cut-off of 75 Hartree was adopted for Brillouin zone sampling.[47] Grimme's DFT-D3 scheme was used for van der Waals dispersion correction.[48] The transmission spectra of the optimized devices were computed by using the non-equilibrium Green function (NEGF) approach as implemented in QuantumATK,[49] and a $5 \times 5 \times 150$ k-point mesh was adopted.

Conflicts of interest

There are no conflicts to declare.

Acknowledgements

This journal is © The Royal Society of Chemistry 2024

J. Mater. Chem. C, 2024, **12**, 60–65 | **63**

References

1 H. Chen and J. Fraser Stoddart, *Nat. Rev. Mater.*, 2021, **6**, 804–828.
2 T. A. Su, M. Neupane, M. L. Steigerwald, L. Venkataraman and C. Nuckolls, *Nat. Rev. Mater.*, 2016, **1**, 16002.
3 D. Xiang, X. Wang, C. Jia, T. Lee and X. Guo, *Chem. Rev.*, 2016, **116**, 4318–4440.
4 W.-Y. Lo, N. Zhang, Z. Cai, L. Li and L. Yu, *Acc. Chem. Res.*, 2016, **49**, 1852–1863.
5 H. Song, M. A. Reed and T. Lee, *Adv. Mater.*, 2011, **23**, 1583–1608.
6 N. Xin, J. Guan, C. Zhou, X. Chen, C. Gu, Y. Li, M. A. Ratner, A. Nitzan, J. F. Stoddart and X. Guo, *Nat. Rev. Phys.*, 2019, **1**, 211–230.
7 W. Lu and C. M. Lieber, *Nat. Mater.*, 2007, **6**, 841–850.
8 J. M. Beebe, B. Kim, J. W. Gadzuk, C. Daniel Frisbie and J. G. Kushmerick, *Phys. Rev. Lett.*, 2006, **97**, 026801.
9 C. Kergueris, J. P. Bourgoin, S. Palacin, D. Esteve, C. Urbina, M. Magoga and C. Joachim, *Phys. Rev. B: Condens. Matter Mater. Phys.*, 1999, **59**, 12505–12513.
10 D. J. Wold and C. D. Frisbie, *J. Am. Chem. Soc.*, 2001, **123**, 5549–5556.
11 B. Xu and N. J. Tao, *Science*, 2003, **301**, 1221–1223.
12 C. J. Muller, J. M. van Ruitenbeek and L. J. de Jongh, *Phys. C*, 1992, **191**, 485–504.
13 B. Huang, X. Liu, Y. Yuan, Z.-W. Hong, J.-F. Zheng, L.-Q. Pei, Y. Shao, J.-F. Li, X.-S. Zhou, J.-Z. Chen, S. Jin and B.-W. Mao, *J. Am. Chem. Soc.*, 2018, **140**, 17685–17690.
14 H. Li, T. A. Su, V. Zhang, M. L. Steigerwald, C. Nuckolls and L. Venkataraman, *J. Am. Chem. Soc.*, 2015, **137**, 5028–5033.
15 M. S. Inkpen, Z. F. Liu, H. Li, L. M. Campos, J. B. Neaton and L. Venkataraman, *Nat. Chem.*, 2019, **11**, 351–358.
16 F. Schwarz, G. Kastlunger, F. Lissel, C. Egler-Lucas, S. N. Semenov, K. Venkatesan, H. Berke, R. Stadler and E. Lörtscher, *Nat. Nanotechnol.*, 2016, **11**, 170–176.
17 F. M. Raymo, *Adv. Mater.*, 2002, **14**, 401–414.
18 L. Bogani and W. Wernsdorfer, *Nat. Mater.*, 2008, **7**, 179–186.
19 Y. Komoto, S. Fujii, M. Iwane and M. Kiguchi, *J. Mater. Chem. C*, 2016, **4**, 8842–8858.
20 Y.-H. Wang, H. Huang, Z. Yu, J.-F. Zheng, Y. Shao, X.-S. Zhou, J.-Z. Chen and J.-F. Li, *J. Mater. Chem. C*, 2020, **8**, 6826–6831.
21 A. K. Ismael, K. Wang, A. Vezzoli, M. K. Al-Khaykanee, H. E. Gallagher, I. M. Grace, C. J. Lambert, B. Xu, R. J. Nichols and S. J. Higgins, *Angew. Chem., Int. Ed.*, 2017, **56**, 15378–15382.
22 S.-L. Lv, C. Zeng, Z. Yu, J.-F. Zheng, Y.-H. Wang, Y. Shao and X.-S. Zhou, *Biosensors*, 2022, **12**, 565.
23 Z. Yu, Y.-X. Xu, J.-Q. Su, P. M. Radjenovic, Y.-H. Wang, J.-F. Zheng, B. Teng, Y. Shao, X.-S. Zhou and J.-F. Li, *Angew. Chem., Int. Ed.*, 2021, **60**, 15452–15458.
24 J.-C. Mao, L.-L. Peng, W.-Q. Li, F. Chen, H.-G. Wang, Y. Shao, X.-S. Zhou, X.-Q. Zhao, H.-J. Xie and Z.-J. Niu, *J. Phys. Chem. C*, 2017, **121**, 1472–1476.
25 P. Moreno-García, M. Gulcur, D. Z. Manrique, T. Pope, W. Hong, V. Kaliginedi, C. Huang, A. S. Batsanov, M. R. Bryce, C. Lambert and T. Wandlowski, *J. Am. Chem. Soc.*, 2013, **135**, 12228–12240.
26 J. Šebera, M. Lindner, J. Gasior, G. Mészáros, O. Fuhr, M. Mayor, M. Valášek, V. Kolivoška and M. Hromadová, *Nanoscale*, 2019, **11**, 12959–12964.
27 X. Zhao, X. Zhang, K. Yin, S. Zhang, Z. Zhao, M. Tan, X. Xu, Z. Zhao, M. Wang, B. Xu, T. Lee, E. Scheer and D. Xiang, *Small Methods*, 2023, **7**, 2201427.
28 S. Kaneko, D. Murai, S. Marqués-González, H. Nakamura, Y. Komoto, S. Fujii, T. Nishino, K. Ikeda, K. Tsukagoshi and M. Kiguchi, *J. Am. Chem. Soc.*, 2016, **138**, 1294–1300.
29 C. Jia and X. Guo, *Chem. Soc. Rev.*, 2013, **42**, 5642–5660.
30 L. Tong, Z. Yu, Y.-J. Gao, X.-C. Li, J.-F. Zheng, Y. Shao, Y.-H. Wang and X.-S. Zhou, *Nat. Commun.*, 2023, **14**, 3397.
31 Y.-H. Wang, X.-C. Li, Z. Yu, J.-F. Zheng and X.-S. Zhou, *Curr. Opin. Electrochem.*, 2023, **39**, 101279.
32 T. Ghomian, O. Kizilkaya, L. K. Domulevicz and J. Hihath, *Nanoscale*, 2022, **14**, 6248–6257.
33 L. Gerhard, K. Edelmann, J. Homberg, M. Valášek, S. G. Bahoosh, M. Lukas, F. Pauly, M. Mayor and W. Wulfhekel, *Nat. Commun.*, 2017, **8**, 14672.
34 I. L. Herrer, A. K. Ismael, D. C. Milán, A. Vezzoli, S. Martín, A. González-Orive, I. Grace, C. Lambert, J. L. Serrano, R. J. Nichols and P. Cea, *J. Phys. Chem. Lett.*, 2018, **9**, 5364–5372.
35 A. Vezzoli, *Nanoscale*, 2022, **14**, 2874–2884.
36 Y.-H. Kim, H. S. Kim, J. Lee, M. Tsutsui and T. Kawai, *J. Am. Chem. Soc.*, 2017, **139**, 8286–8294.
37 R. Stadler, K. S. Thygesen and K. W. Jacobsen, *Phys. Rev. B: Condens. Matter Mater. Phys.*, 2005, **72**, 241401.
38 M. Kiguchi, T. Ohto, S. Fujii, K. Sugiyasu, S. Nakajima, M. Takeuchi and H. Nakamura, *J. Am. Chem. Soc.*, 2014, **136**, 7327–7332.
39 Z. Zhu, H. Qu, Y. Chen, C. Zhang, R. Li, Y. Zhao, Y. Zhou, Z. Chen, J. Liu, Z. Xiao and W. Hong, *J. Mater. Chem. C*, 2021, **9**, 16192–16198.
40 C. Seth, V. Kaliginedi, S. Suravarapu, D. Reber, W. Hong, T. Wandlowski, F. Lafolet, P. Broekmann, G. Royal and R. Venkatramani, *Chem. Sci.*, 2017, **8**, 1576–1591.
41 M. Mennicken, S. K. Peter, C. Kaulen, U. Simon and S. Karthäuser, *J. Phys. Chem. C*, 2019, **123**, 21367–21375.
42 L. Palomino-Ruiz, P. Reiné, I. R. Márquez, I. Álvarez de Cienfuegos, N. Agraït, J. M. Cuerva, A. G. Campaña, E. Leary, D. Miguel, A. Millán, L. A. Zotti and M. T. González, *J. Mater. Chem. C*, 2021, **9**, 16282–16289.
43 X. Pan, B. Lawson, A. M. Rustad and M. Kamenetska, *Nano Lett.*, 2020, **20**, 4687–4692.
44 M. S. José, A. Emilio, D. G. Julian, G. Alberto, J. Javier, O. Pablo and S.-P. Daniel, *J. Phys.: Condens. Matter*, 2002, **14**, 2745.
45 S. Smidstrup, T. Markussen, P. Vancraeyveld, J. Wellendorff, J. Schneider, T. Gunst, B. Verstichel, D. Stradi, P. A. Khomyakov, U. G. Vej-Hansen, M.-E. Lee, S. T. Chill, F. Rasmussen, G. Penazzi, F. Corsetti, A. Ojanperä, K. Jensen, M. L. N. Palsgaard, U. Martinez, A. Blom, M. Brandbyge and K. Stokbro, *J. Phys.: Condens. Matter*, 2020, **32**, 015901.

46 J. P. Perdew, K. Burke and M. Ernzerhof, *Phys. Rev. Lett.*, 1996, **77**, 3865–3868.

47 H. J. Monkhorst and J. D. Pack, *Phys. Rev. B: Solid State*, 1976, **13**, 5188–5192.

48 S. Grimme, J. Antony, S. Ehrlich and H. Krieg, *J. Chem. Phys.*, 2010, **132**, 154104.

49 M. Brandbyge, J.-L. Mozos, P. Ordejón, J. Taylor and K. Stokbro, *Phys. Rev. B: Condens. Matter Mater. Phys.*, 2002, **65**, 165401.

This journal is © The Royal Society of Chemistry 2024

J. Mater. Chem. C, 2024, **12**, 60–65 | **65**